JOURNAL OF THE KOREAN INSTITUTE OF ELECTROMAGNETIC ENGINEERING AND SCIENCE, VOL. 12, NO. 1, 70~76, MAR. 2012

http://dx.doi.org/10.5515/JKIEES.2012.12.1.70
ISSN 2234-8395 (Online) · ISSN 2234-8409 (Print)

Comparison of Detection Probability for Conventional and Time-Reversal (TR) Radar Systems

Hyung-Ha Yoo[1] · Il-Suek Koh[2]

Abstract

We compare the detection probabilities of the time-reversal(TR) detection system and the conventional radar system. The target is assumed to be hidden inside a random medium such as a forest. We propose a TR detection system based on the SAR(Synthetic Aperture Radar) algorithm. Unlike the conventional SAR images, the proposed TR-SAR system has an interesting property. Specifically, the target-related signal components due to the time-reversal refocusing characteristics, as well as some of clutter-related signal components are concentrated at the time-reversal reference point. The remaining clutter-related signal components are scattered around that reference point. In this paper, we model the random media as a collection of point scatterers to avoid unnecessary complexities. We calculate the detection probability of the TR radar system based on the proposed simple random media model.

Key words: Time-Reversal, Target Detection, SAR, TR-SAR, Detection Probability.

Ⅰ. Introduction

For energy transmission, negative effects such as signal scattering and attenuation are unavoidable. Various methods have been suggested to overcome these effects including the TR technique. This technique is one of those that exploits the multipath characteristic of the random inhomogeneous media to restore the original signal [1], [2].

The TR technique can be explained in the following way. First, a signal is emitted from a transmitter and propagates through a random media to arrive at a receiver. The received signal is then time-reversed and re-emitted to experience the same random medium. Next, the time-reversed signal can be temporally and spatially refocused at the original transmitter. This TR technique is very similiar to phase conjugation in nonlinear optics [3].

The applicability of the TR technique was first investigated in acoustics [4], [5]. This was followed by the experimental validation to show the TR technique could also be applied to the microwave field [6]. Currently, various applications are being studied including microwave imaging, and SAR, among others [7]~[9].

In this paper, we characterize the target detection scheme using SAR system, when a target is inside a random medium. It has the following procedure. First, as with a conventional SAR procedure, the SAR system emits a signal and receives its echo from the target and the clutter at each point on the synthetic aperture line. We indicate the raw data from this procedure as A.

Second, we choose a suspicious region, where a target might be located. We indicate the center of the suspicious region as a TR reference point. We then reverse the signal in a time domain with respect to this reference point. We indicate the signal data from this procedure as B. We re-emit the TR signal to obtain the finally received signal at each point on the synthetic aperture line, which is mathematically equivalent to taking the signal A matched filtered with the signal B. Then, we obtain the TR-SAR image by applying a proper SAR algorithm. We model the random media as a collection of points as seen in Fig. 1.

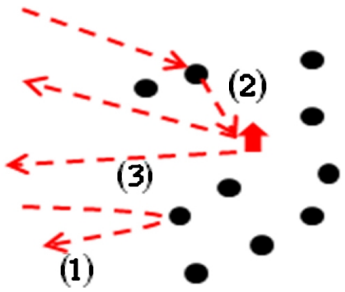

Fig. 1. Scattering environment. (1) clutter scattering, (2) clutter-target scattering, (3) target LOS(Line-Of-Sight).

Manuscript received August 25, 2011 ; Revised February 2, 2012 ; Accepted February 16, 2012. (ID No. 20110825-05J)
[1]Graduate School of Information & Telecommunication. Inha University, Incheon, Korea.
[2]Dept. of Electronic Engineering, Inha University, Incheon, Korea.
Corresponding Author : Il-Suek Koh (e-mail : ikoh@inha.ac.kr)

Fig. 1 shows that the scattering environment based on the proposed random media model. (1) is a signal component, directly scattered by a point clutter. (2) is a multipath component via the target and a point clutter; and (3) is a target LOS component. In conventional radar system, only (3) is devoted to the target-related signal, whereas the others are all devoted to the noise-related signal. However, (3) as well as (2) are contributors to the target-related signal in the TR-SAR scheme. In section II, we describe the TR-SAR and its image property and explain how this TR-SAR scheme can be used to detect a target. In section III, we estimate the probability distribution function(pdf) of the TR signal plus noise to compute the detection and false alarm probabilities of the TR detection system. We then compare the detection probability of the TR system with the conventional system.

Ⅱ. The TR-SAR System

In this section, we describe the TR-SAR image characteristics and show its utilization as a TR detection system.

Fig. 2 shows the TR-SAR scheme considered in the paper, where η is the azimuth time, V and h are the SAR vehicle's speed and the vehicle's height, respectively, (x_i, y_i, z_i) are the coordinates of the i^{th} clutter, (x_0, y_0, z_o) are the coordinates of the target, and (x_r, y_r, z_r) are the coordinates of the TR reference point. If the SAR system emits the signal, its echo consists of the three signal components according to Fig. 1.

$$A_1 = \sum_{i=1}^{N} c_i rect\left(\frac{t-2t_i'}{T}\right) e^{i[2\pi f_0(t-2t_i')+\pi\gamma(t-2t_i')^2]} \quad (1)$$

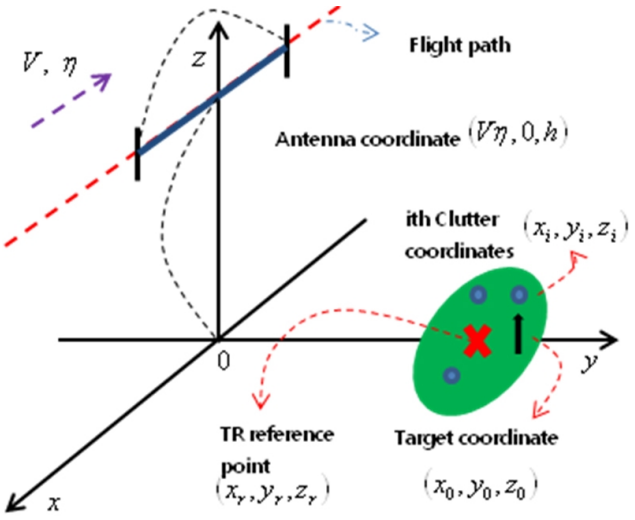

Fig. 2. Considered TR-SAR scheme.

$$A_2 = \sum_{i=1}^{N} d_i rect\left(\frac{t-t_i-t_0'}{T}\right) e^{i\left[2\pi f_0(t-t_i-t_0')+\pi\gamma(t-t_i-t_0')^2\right]} \quad (2)$$

$$A_3 = b_0 rect\left(\frac{t-2t_0'}{T}\right) e^{i\left[2\pi f_0(t-2t_0')+\pi\gamma(t-2t_0')^2\right]} \quad (3)$$

A_1 is the echo due to the direct clutter scattering, A_2 is the echo due to the target and clutter multiple scattering, and A_3 is the echo due to the target LOS. A chirp waveform is chosen. f_0 is the carrier frequency, where γ is the chirp rate. N is the number of clutters in the random medium, b_0 is the target reflectivity, c_i is the clutter reflectivity of the i^{th} clutter, and d_i is the scattering coefficient for the i^{th} clutter and target multiple scattering. As explained in section I, the signal components (1), (2), and (3) are the signal A. The signal components after the TR process become the signal B. The final TR-SAR image can be obtained by applying the matched filter between A and B in range, followed by azimuth filtering. Nine image components then appear for one point target. Their coordinates and magnitude are listed in the Table 1.

In Table 1, $R_{r0} = \sqrt{y_r^2 + (h-z_r)^2}$, $R_{00} = \sqrt{y_0^2 + (h-z_0)^2}$ and $R_{i0} = \sqrt{y_i^2 + (h-z_i)^2}$. $R_{i0}' = R_{i0} + \alpha_i$, where α_i is the distance between the target and the i^{th} clutter, $\alpha_i = \sqrt{(x_i-x_0)^2 + (y_i-y_0)^2 + (z_i-z_0)^2}$. From Table 1, we can observe an interesting property that when $i=k$, the image components S_{11}, S_{22}, and S_{33} are all coherently added at

Table 1. TR-SAR image components.

	Range	Azimuth	Magnitude
S_{11}	$R_{r0} - R_{k0} + R_{i0}$	$x_r - x_k + x_i$	$\sum_{i=1}^{N}\sum_{k=1}^{N} c_i c_k^*$
S_{12}	$R_{r0} - \frac{R_{k0}'}{2} - \frac{R_{00}}{2} + R_{i0}$	$x_r - \frac{x_k}{2} - \frac{x_0}{2} + x_i$	$\sum_{i=1}^{N}\sum_{k=1}^{N} c_i d_k^*$
S_{13}	$R_{r0} - R_{00} + R_{i0}$	$x_r - x_0 + x_i$	$\sum_{i=1}^{N} c_i b_0^*$
S_{21}	$R_{r0} - R_{k0} + \frac{R_{i0}'}{2} + \frac{R_{00}}{2}$	$x_r - x_k + \frac{x_i}{2} + \frac{x_0}{2}$	$\sum_{i=1}^{N}\sum_{k=1}^{N} d_i c_k^*$
S_{22}	$R_{r0} - \frac{R_{k0}'}{2} + \frac{R_{i0}'}{2}$	$x_r - \frac{x_k}{2} + \frac{x_i}{2}$	$\sum_{i=1}^{N}\sum_{k=1}^{N} d_i d_k^*$
S_{23}	$R_{r0} - \frac{R_{00}}{2} + \frac{R_{i0}'}{2}$	$x_r - \frac{x_0}{2} + \frac{x_i}{2}$	$\sum_{i=1}^{N} d_i b_0^*$
S_{31}	$R_{r0} - R_{k0} + R_{00}$	$x_r - x_k + x_0$	$\sum_{k=1}^{N} b_0 c_k^*$
S_{32}	$R_{r0} - \frac{R_{k0}'}{2} + \frac{R_{00}}{2}$	$x_r - \frac{x_k}{2} + \frac{x_0}{2}$	$\sum_{k=1}^{N} b_0 d_k^*$
S_{33}	R_{r0}	x_r	$\lvert b_0\rvert^2$

the coordinates of the TR reference point in the SAR image space, (R_{r0}, x_r). All other components are scattered around that TR reference point. For the detection probability of the TR-SAR, the magnitudes of S_{11}, S_{22} and S_{33} are important, and are summarized as:

$$S_{11}(i=k)=\sum_{i=1}^{N}|c_i|^2 A(x-x_r)R\left(t-\frac{2}{c}R_{r0}\right) \quad (4)$$

$$S_{22}(i=k)=\sum_{i=1}^{N}|d_i|^2 A(x-x_r)R\left(t-\frac{2}{c}R_{r0}\right) \quad (5)$$

$$S_{33}(i=k)=|b_0|^2 A(x-x_r)R\left(t-\frac{2}{c}R_{r0}\right) \quad (6)$$

Eqn. (4) is caused by the direct scattering of the clutters, while (5) is caused by the multiple scattering of the clutters and the target and, (6) is only caused by the LOS component of the target. If a target exists, (4), (5) and (6) are all added at the TR-reference point. If a target does not exist, only (4) appears at the TR-reference point.

Fig. 3 simply shows the TR-SAR detection scheme: (a) shows the suspicious region and (b) is its corresponding raw SAR data. Therefore, after designating a TR reference point in the middle of the suspicious region, we cut the signal in range direction (with the width of a in this figure). We then reverse the cut signal in time and re-emit it to obtain the TR-SAR image of corresponding region. The image will show the different magnitudes depending on the absence or the presence of the target in the suspicious region. With this method, as explained so far, we can say whether a tar-

(a) Physical space

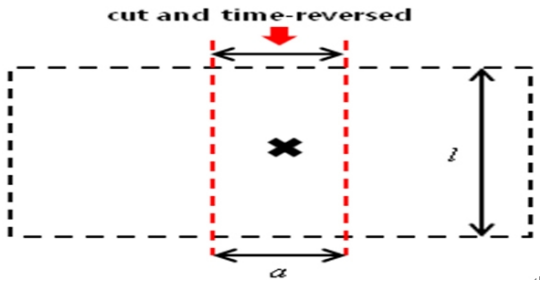

(b) Raw data corresponding to the physical space (a)

Fig. 3. TR-SAR detection scheme.

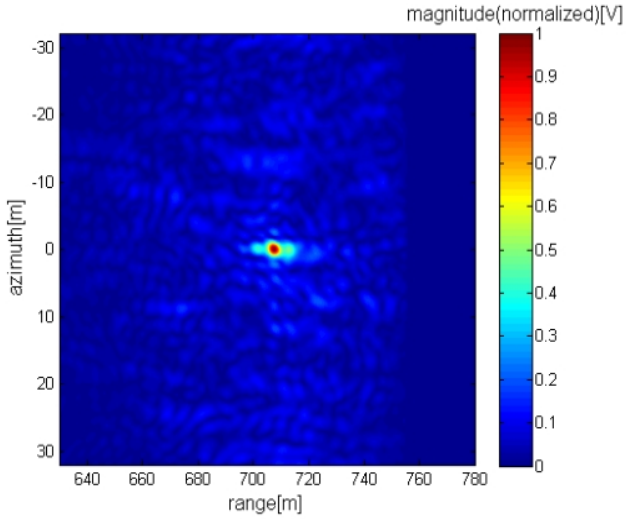

(a) The image when a target is present

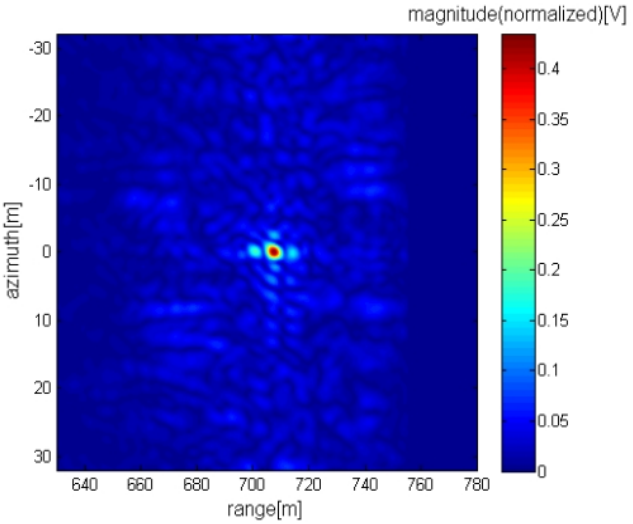

(b) The image when a target is absent

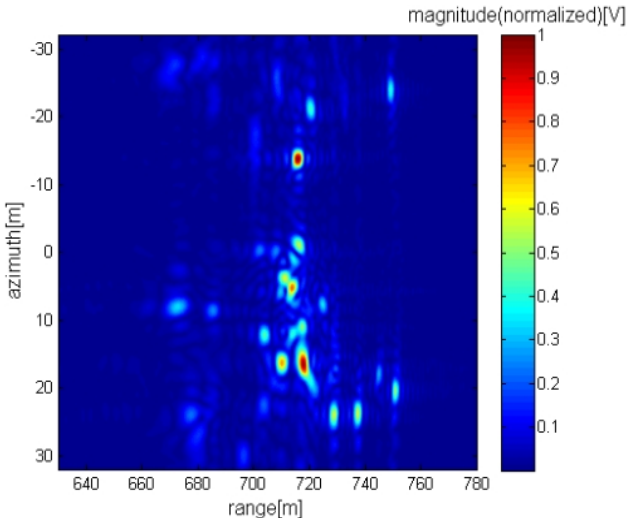

(c) The corresponding conventional SAR image when the target exists

Fig. 4. TR-SAR images.

get is in the box shaped region of dimension a by l.

Fig. 4 shows the simulation results of TR-SAR images and the conventional image. The intensity of (a) and (c) are normalized to 1. The intensity scaling of (b) is done associated with (a) for the direct comparison. For the simulation, we generate 30 point clutters within the boundary of a box-shaped region whose dimension is 100×100×10 meters. A target is laid on the bottom center of that box. c_i, d_i are generated using complex Gaussian random numbers, whose variances are equally 0.198. The value of 0.198 is converted from one value of RCS for a jack pine tree, -11.0 dBsm[10]. We use a chirp waveform and a carrier frequency of 1 GHz. The vehicle speed is 320 m/s. The length of synthetic aperture line is 60 m. A target is situated at $(707,0)$ m in the image space. The TR reference point is set to have equal coordinates of the target for the sake of convenience. The signal is cut with a width $a = 60$ m (see Fig. 3) and time-reversed. In Fig. 4, (a) is the case when a target is present; (b) is the case when a target is absent. (c) is the conventional image when the target exists. All three of (a), (b) and (c) are obtained from the same parameters. The target is completely obscured by ghost images in (c). The magnitude of (a) is almost twice as much as the magnitude of (b). This indicates that this TR-SAR scheme works as a target detection system if we concentrate on the image component converged at the TR reference point.

Ⅲ. Detection Probability of TR-SAR Detection System

As described in the previous section, two different images are coherently added at the TR reference point: target and clutter. To calculate the detection probability of the proposed TR-SAR system, we should compute the pdf of the target plus noise. If we model the reflection and the multiple scattering coefficients as (7), (8) and (9), complex Gaussian random variables with zero mean, the magnitude of image component at the TR reference point can be written as (10), (11).

$$c_i = c_{ix} + ic_{iy}, \quad d_i = d_{ix} + id_{iy} \tag{7}$$

$$c_{ix} = c_{iy} = N\left(0, {\sigma_c}^2\right) \tag{8}$$

$$d_{ix} = d_{iy} = N\left(0, {\sigma_t}^2\right) \tag{9}$$

$$|b_0|^2 + \sum_{i=1}^{N} {d_{ix}}^2 + {d_{iy}}^2 \tag{10}$$

$$\sum_{i=1}^{N} {c_{ix}}^2 + {c_{iy}}^2 \tag{11}$$

Eqn. (10) is the magnitude contribution of target-like components which correspond to S_{22}, S_{33} in Table 1. Eqn. (11) is the magnitude contribution of noise-like component which corresponds to S_{11} in Table 1. Both (10) and (11) are the sum of Gaussian random number squared. Hence, the pdf of (10) and (11) becomes a Chi-square distribution as

$$f_t(y) = \frac{1}{{\sigma_t}^2 2^N \Gamma(N)} \left(\frac{y - |b_0|^2}{{\sigma_t}^2} \right)^{N-1} e^{-\frac{y-|b_0|^2}{2{\sigma_t}^2}} \tag{12}$$

$$f_t(y) = \frac{1}{{\sigma_c}^2 2^N \Gamma(N)} \left(\frac{y}{{\sigma_c}^2} \right)^{N-1} e^{-\frac{y}{2{\sigma_c}^2}} \tag{13}$$

where y denotes the amplitude of the signal. Eqn. (12) is the pdf for the target-like components. Eqn. (13) is the pdf for the noise-like component. To calculate the detection probability of a target, we need the pdf of the target signal plus noise which can be obtained by performing a convolution between (12) and (13). However, this is rather complicated. Therefore, in this paper, we only provide the numerical results. In Fig. 1, both multiple scattering components (2) and target LOS component (3) contribute to the target-like components in the TR-SAR image. The clutter scattering components (1) contribute to the noise-like components in the TR-SAR image. However, in a conventional radar system, only the target LOS component (3) contributes to the target signal. All other components contribute to the noise. In this paper, we use the Rayleigh distribution for the noise pdf and therefore the pdf of the target plus noise will be the Rician distribution.

$$|b_0|^2 + 2N\left({\sigma_c}^2 + {\sigma_t}^2\right) \tag{14}$$

$$2{\sigma_N}^2 = 2N\left({\sigma_c}^2 + {\sigma_t}^2\right) \tag{15}$$

Eqn. (14) is the power of the conventional radar echo based on the model explained in Fig. 1. From (15), we can estimate the variance of the noise for the conventional radar system. Therefore, the noise and the target plus the noise pdf for the conventional radar system can be written as (16) and (17), respectively.

$$f_N(y) = \frac{y}{{\sigma_N}^2} e^{-\frac{y^2}{2{\sigma_N}^2}} \tag{16}$$

$$f_{N+T}(y) = \frac{y}{{\sigma_N}^2} e^{-\frac{y^2+|b_0|^2}{2{\sigma_N}^2}} I_0\left(\frac{y|b_0|}{{\sigma_N}^2} \right) \tag{17}$$

In (17), $I_0(\cdot)$ is the modified Bessel function of the 0^{th} order. For the direct comparison of the conventional

radar system and the TR-SAR detection system, we normalize the echoed power. If we say y_1 is the amplitude random variable for the target-like components and y_2 is the amplitude random variable for the noise-like components, the total echoed power at the TR reference point of the TR-SAR system becomes (18).

$$P = 4\left(\sigma_c^{\,2} + \sigma_t^{\,2}\right)^2 M^2 + 4|b_0|^2\left(\sigma_c^{\,2} + \sigma_t^{\,2}\right)M + |b_0|^4 \tag{18}$$

$$\begin{aligned} P &= \mathrm{var}\{y_1 + y_2\} + \left|\langle y_1 + y_2\rangle\right|^2 \\ &= \mathrm{var}\{y_1\} + \mathrm{var}\{y_2\} + \mathrm{cov}(y_1, y_2) + \left|\langle y_1 + y_2\rangle\right|^2 \end{aligned} \tag{19}$$

Eqn. (18) is calculated based on (19). For the power normalization, equating (14) with (18), (20) is obtained.

$$M = \frac{1}{2\left(\sigma_c^{\,2} + \sigma_t^{\,2}\right)}\left(-|b_0|^2 + \sqrt{|b_0|^2 + 2N\left(\sigma_c^{\,2} + \sigma_t^{\,2}\right)}\right) \tag{20}$$

Hence, by using M instead of N in (12) and (13), the power normalization is completed. We assume that noise pdf follows the Rayleigh distribution for the conventional radar. Then, with a given false alarm probability, the threshold value is calculated as (21)

$$\begin{aligned} P_{FA} &= \int_T^\infty \frac{y}{\sigma_N^{\,2}} e^{-\frac{y^2}{2\sigma_N^{\,2}}} dy = e^{-\frac{T^2}{2\sigma_N^{\,2}}} \\ T &= \sigma_N \sqrt{2\log\frac{1}{P_{FA}}} \end{aligned} \tag{21}$$

However, this threshold value becomes useless if the SNR is too low because the noise pdf and the target plus the noise pdf almost will overlap. We compare the detection probability of the conventional radar system with the TR-SAR detection system. We magnify the performance of the TR-SAR detection system by choosing a rather small target reflectivity, $b_0 = 10^{-3}$. We set $\sigma_c = 0.198$ excerpted from [10]. N is the number of clutter that is chosen to be 100.

Fig. 5 shows the pdf of the target, clutter, target plus clutter of the conventional and TR-SAR detection system. The value of σ_t stands for the degree of the time-reversal effect. A larger value gives a larger time-reversal effect. In Fig. 5, we consider three cases, $\sigma_t = 0.6\sigma_c$, $\sigma_t = 1.0\sigma_c$ and compare their differences. As shown in Fig. 5, the pdf of the noise and the target plus noise of the conventional system almost overlap due to a very low SNR in all three cases. For the case of the TR-SAR detection system, we can observe that the pdf of the target plus noise is shifted away from the pdf of the noise as the value of σ_t increases. This indicates that the value of detection probability goes up as TR effect increases.

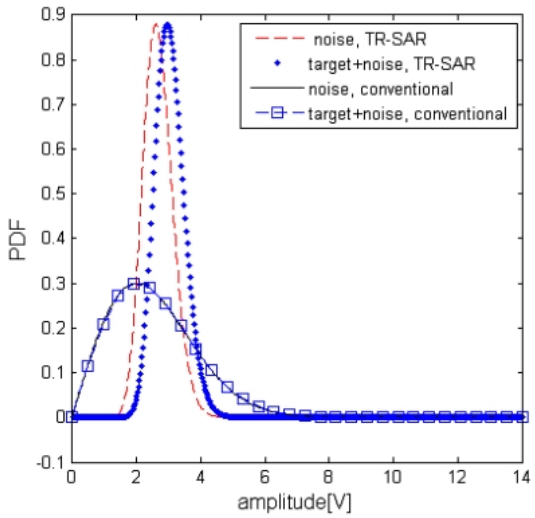

(a) $\sigma_t = 0.2\sigma_c$

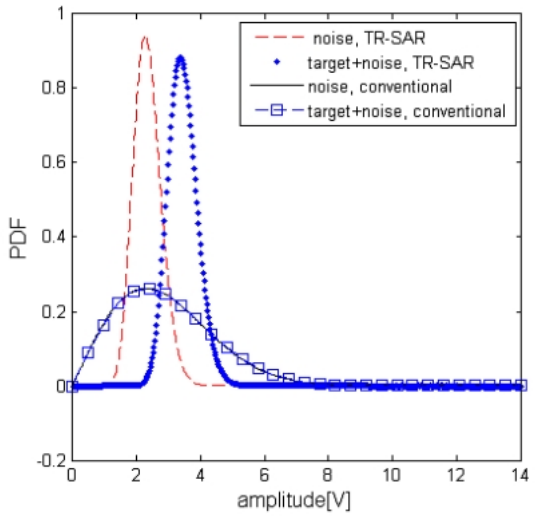

(b) $\sigma_t = 0.6\sigma_c$

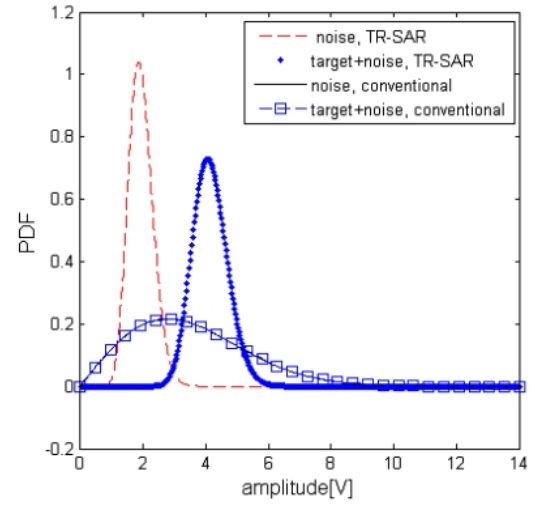

(c) $\sigma_t = 1.0\sigma_c$

Fig. 5. Pdf of noise, noise plus target of the conventional and TR-SAR detection system.

Table 2. Detection and false alarm probabilities of the conventional and TR-SAR detection scheme.

σ_t	SNR	TR-SAR detection		Conventional system	
		P_D	P_{FA}	P_D	P_{FA}
$0.2\sigma_c$	0.0096	0.7021	0.3794	0.3859	0.3823
$0.6\sigma_c$	0.0074	0.9136	0.1177	0.4645	0.4619
$1.0\sigma_c$	0.0050	0.9913	0.0099	0.5714	0.5698

Table 2 shows the detection probabilities and the false alarm probabilities of the TR-SAR detection system and the conventional system for three values of σ_t. The threshold value T is chosen to be the point where the noise pdf and the target plus noise pdf of the TR-SAR system intersect. Table 2 shows that detection probability goes up and the false alarm probability falls as σ_t increases for the TR-SAR detection scheme. On the other hand, the detection probability and the false alarm probability of the conventional system in each case remain virtually same. This indicates that it is almost impossible to detect a target with this conventional system when the SNR is very low.

Fig. 6 shows the detection probabilities and the false alarm probabilities of the TR-SAR detection system. We draw three curves as the function of SNR with different σ_t to reflect the degrees of time-reversal effect. As expected, a larger time-reversal effect results in high detection probability and low false alarm probability even

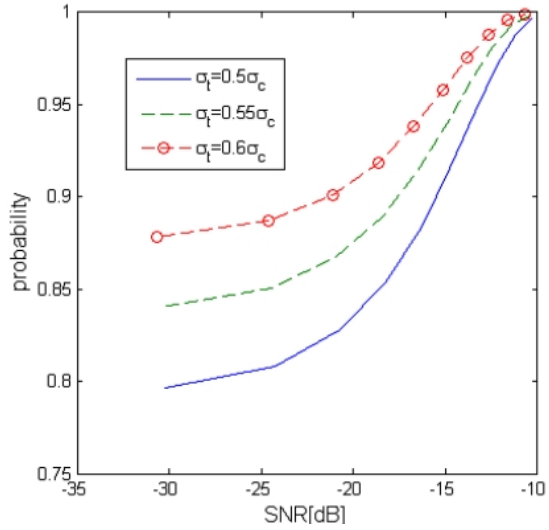

(a) Detection probabilities

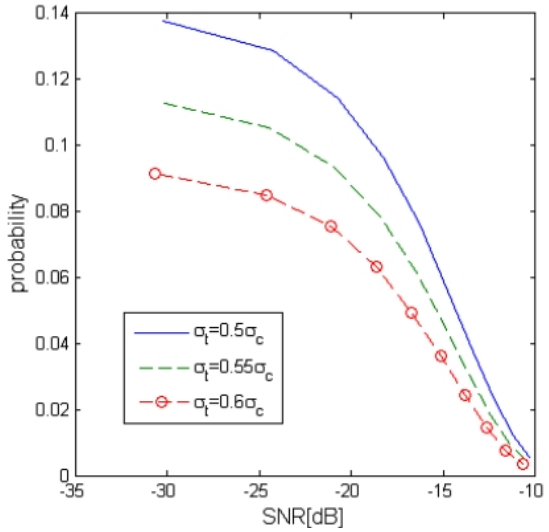

(b) False alarm probabilities

Fig. 6. Values of detection and false alarm probabilities as the function of SNR.

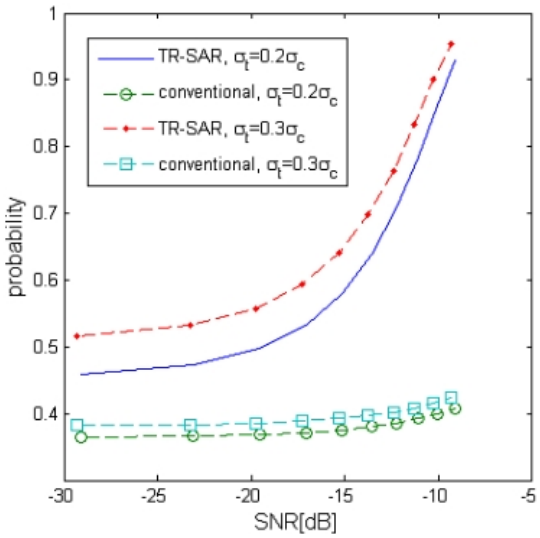

(a) Detection probabilities

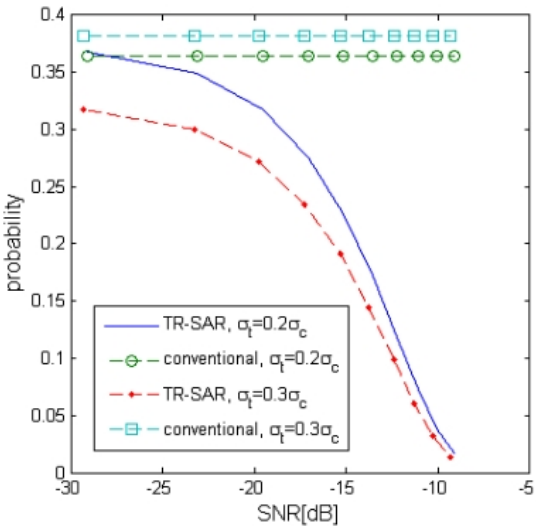

(b) False alarm probabilities

Fig. 7. Comparison of the TR-SAR detection system with the conventional radar system.

if the SNR is very low.

Fig. 7 shows the comparison of the TR-SAR detection scheme with the conventional scheme: (a) denotes the comparison of the detection probabilities, while (b) denotes the comparison of the false alarm probabilities. It is clear from this figure that the TR-SAR detection scheme works fine even if SNR is low.

Ⅳ. Conclusion

A rich scattering environment results in many negative effects, such as low detection probability, and ghost images, among others. In this paper, we combine the TR technique with the SAR technique to propose the TR-SAR detection scheme. We confirm that the detection probability goes up and the false alarm probability falls depending on the degrees of the time-reversal effect. The most important feature of this scheme is that even when the SNR is very low, the TR-SAR detection scheme shows a reasonably high detection probability and low false alarm probability. In a similar situation, the conventional detection scheme does not work.

This research was supported by DAPA(Defence Acquisition Program Administration) and ADD(Agency for Defence Development (contract number, UD-100002KD).

References

[1] M. Fink, "Time-reversal ultrasonic fields-part I: basic principles," *IEEE Trans. Ultrason. Ferroelectr., Freq. Control*, vol. 39, no. 5, pp. 555-566, May 1992.

[2] F. Wu, J. L. Thomas, and M. Fink, "Time-reversal ultrasonic fields-part Ⅱ: Experimental results," *IEEE Trans. Ultrason. Ferroelectr., Freq. Control*, vol. 39, no. 5, pp. 567-578, May 1992.

[3] E. Hecht, *Optics*, 4th Edition, Addison Wesley, pp. 230-232, 2002.

[4] M. Fink, G. Montaldo, and M. Tanter, "Time-reversal acoustics," *Ultrason. Ferroelectr., Freq. Control Joint 50th Anniversary Conference*, pp. 850-859, 2004.

[5] A. Derode, P. Roux, and M. Fink, "Robust acoustic time reversal with high-order multiple scattering," *Physical Review Letters*, vol. 75, no. 23, pp. 4206-4209, 1995.

[6] G. Lerosey, J. de Rosny, A. Tourin, A. Derode, G. Montaldo, and M. Fink, "Time-reversal of electromagnetic waves," *Physical Review Letters*, vol. 92, no. 19, pp. 193904-1-193904-3, May 2004.

[7] Y. Jin, J. M. F. Moura, and N. O'donoughue, "Time reversal synthetic aperture radar imaging in multipath," *ACSSC 2007*, Nov. 2007.

[8] D. Liu, J. Krolik, and L. Carin, "Electromagnetic target detection in uncertain media: time-reversal and minimum-variance algorithms," *IEEE Trans. on Geosciences and Remote Sensing*, vol. 45, no. 4, pp. 934-944, Apr. 2007.

[9] D. Liu, G. Kang, L. Li, Y. Chen, S. Vasudevan, W. Joines, Q. Huo Liu, J. Krolik, and L. Carin, "Electromagnetic time-reversal imaging of a target in a cluttered environment," *IEEE Trans. on Geosciences and Remote Sensing*, vol. 53, no. 9, pp. 3058-3066, Sep, 2005.

[10] D. R. Sheen, L. P. Johnson, "Statistical and spatial properties of forest clutter measured with polarimetric synthetic aperture radar (SAR)," *IEEE Trans. on Geosciences and Remote Sensing*, vol. 30, no. 30, May 1992.

[11] M. Sekine, Y. Mao, *Weibull Radar Clutter*, Peter Peregrinus Ltd., pp. 4-47, 1990.

Hyung-Ha Yoo

was born in Seoul, South Korea in 1977. He received B.S. degree in physics from Inha University, Incheon, South Korea in 2004. He worked as a mathematics lecturer in a private mathematics Institute for three years. He has been a Ph.D. candidate student since 2007. His research interests include time-reversal signal processing, SAR system, nonlinear optics.

Il-Suek Koh

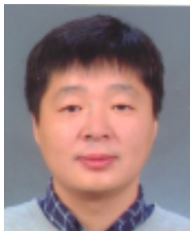

(M'02) was born in South Korea. He received the B.S. and M.S. degrees in electronics engineering from Yonsei University, Seoul, South Korea, in 1992 and 1994, respectively, and the Ph.D. degree from the University of Michigan at Ann Arbor, in 2002. In 1994, he entered LG Electronics Ltd., Seoul, as a research engineer. Currently, he is an associate professor at Inha University, Incheon, South Korea. His research interests include wireless communication channel modeling and numerical and analytical techniques for electromagnetic field propagation.